Anisotropic Elasticity of Quasi-One-Component Polymer Nanocomposites

Panayiotis Voudouris,[†,#] Jihoon Choi,[‡,#] Nikos Gomopoulos,[§] Rebecca Sainidou,[⊥] Hongchen Dong,[¶] Krzysztof Matyjaszewski,[¶] Michael R. Bockstaller,[‡,*] and George Fytas[†,§,*]

[†]Departments of Chemistry and Materials Science & Technology, University of Crete and FORTH, P.O Box 71110, Heraklion, Greece, [‡]Department of Materials Science and Engineering, Carnegie Mellon University, 5000 Forbes Avenue, Pittsburgh, Pennsylvania 15213, United States, [§]Max Planck Institute for Polymer Research, Ackermannweg 10, 55128 Mainz, Germany, [⊥]Laboratoire Ondes et Milieux Complexes FRE CNRS 3102, Université du Havre, Place R. Schuman, 76610 Le Havre, France, and [¶]Department of Chemistry, Carnegie Mellon University, 4400 Fifth Avenue, Pittsburgh, Pennsylvania 15213, United States. [#]These authors contributed equally to this work.

ABSTRACT The in-plane and out-of-plane elastic properties of thin films of "quasi-one-component" particle-brush-based nanocomposites are compared to those of "classical" binary particle—polymer nanocomposite systems with near identical overall composition using Brillouin light scattering. Whereas phonon propagation is found to be independent of the propagation direction for the binary particle/polymer blend systems, a pronounced splitting of the phonon propagation velocity along the in-plane and out-of-plane film direction is observed for particle-brush systems. The anisotropic elastic properties of quasi-one-component particle-brush systems are interpreted as a consequence of substrate-induced order formation into layer-type structures and the associated breaking of the symmetry of the film. The results highlight new opportunities to engineer quasi-one-component nanocomposites with advanced control of structural and physical property characteristics based on the assembly of particle-brush materials.

KEYWORDS: Brillouin light scattering · particle brush · nanocomposite · elasticity · self-assembly

The potential to impart novel and enhanced properties to polymer materials without sacrificing the advantageous formability of the polymer matrix has fueled both academic and industrial interest in polymer nanocomposites during the past 20 years.[1−7] For example, particle fillers are used to enhance thermo-mechanical properties or to engineer tailored electrical, optical, or transport properties of polymer thin films for applications ranging from electronic packaging to barrier and protective coatings.[8−13] Although the details of how a physical property is affected by the presence of particle fillers is dependent on the nature of the underlying interactions, a common observation is that properties of polymer nanocomposites intimately depend on the morphology of the particle dispersion.[14] To establish the governing parameters that control dispersion morphologies as well as process strategies to facilitate the engineering of prescribed morphologies is thus a focal point of nanocomposite research.[15−19] In many instances, such as for the modulation of optical, dielectric, or thermo-mechanical properties, uniform particle dispersions are typically desired in order to prevent scattering, conductive pathways, or to efficiently capitalize on interfacial interactions. Applications deriving from these properties are therefore often linked to the ability of fabricating uniform particle dispersions at high concentrations of the inorganic component. In athermal particle/polymer blends this presents a formidable challenge because entropic interactions (typically) counteract particle dispersion for the majority of technologically relevant composite formulations.[20] The need for viable routes for the preparation of thermodynamically stable, uniform, and concentrated particle dispersions has motivated research in alternative strategies of nanocomposite preparation.

One promising path toward thermodynamic stable particle dispersions with controlled microstructure is based upon the grafting of polymer chains to the surface of particles and the subsequent assembly of the polymer-grafted particles (in the following denoted "particle brushes") into array structures. Polymer-like mechanical characteristics of the particle-brush assembly can be expected if the architecture of the polymer shell allows for substantial chain entanglements.[21] Conditions to realize chain entanglements can be evaluated by considering the conformational transitions of chains grafted to a particle surface. In general, densely polymer-grafted particles are categorized depending on the polymer grafting density and degree of polymerization.[22,23] In the limit of high grafting densities, the concentrated particle-brush (CPB) regime is observed when segmental interactions give rise to extended chain

* Address correspondence to bockstaller@cmu.edu, fytas@mpip-mainz.mpg.de.

Received for review April 18, 2011 and accepted June 20, 2011.

Published online June 20, 2011
10.1021/nn201431w

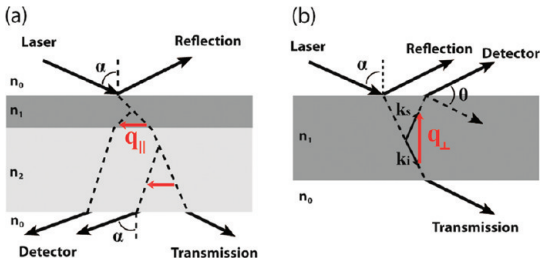

Figure 1. Illustration of scattering geometry. (a) Transmission scattering geometry for recording spectra from a supported film on transparent substrate at a scattering angle twice the incidence angle α. The scattering wave vector q is parallel to the film surface. (b) Reflection scattering geometry. The optical path of the incident and scattered light in a film at a scattering angle $\theta = \pi - 2\alpha$ where α is the angle of incidence. The scattering wave vector q is perpendicular to the film surface.

conformations. As the chain density decreases a transition to the semidilute particle-brush (SDPB) regime is observed in which reduced segmental interactions give rise to more relaxed chain conformations.[24,25] On the basis of this CPB/SDPB model, polymer-like mechanical properties of particle-brush assemblies can be expected if the length of the relaxed segments of the grafted chains exceeds the critical segment length for entanglements. Recent studies have documented the potential of particle-brush systems in the SDPB regime to assemble into quasi-one-component nanocomposites with polymer-like thermomechanical properties. In particular, Vaia and co-workers reported the bottom-up synthesis of nanocomposites by assembly of sparse grafted particle systems that exhibit polymer-type elasticity despite a high filling fraction of inorganic particles (~60 wt %).[26] More recently, Choi *et al.* reported that the grafting of polymeric chains can facilitate the formation of (short-range) ordered yet plastic-compliant particle array structures in which chain entanglements give rise to increased mechanical strength and fracture through polymer-like crazing processes.[21] However, while these previous studies have established the principal feasibility of particle–brush based nanocomposites with polymer-like mechanical attributes, the implications of the architecture of the particle-brush constituents on the interactions and properties of the nanocomposites remain an open question. This is of significant relevance to not only the development of advanced particle-based nanocomposite materials but also the fundamental understanding of the interrelationship between molecular architecture, interactions, and properties of polymer nanocomposite materials.

In this contribution the in-plane and out-of-plane elastic properties (*i.e.*, the mechanical moduli parallel and normal to the film surface at hypersonic frequencies) of thin films of particle brush-based nanocomposites are compared to those of classical binary particle–polymer blend systems with near identical overall composition using Brillouin light scattering (BLS) performed in transmission and reflection mode as depicted in Figure 1. This technique utilizes inelastic scattering of incident laser light by thermally activated hypersonic (GHz) elastic (acoustic) waves in the matter. By analyzing the spectral composition of the inelastically scattered light, the information about the elastic wave propagation and hence the elastic properties of the film can be obtained. The two scattering geometries of Figure 1 allow the selective probing of the phonon propagation with wave vector either parallel ($\mathbf{q} = q_{\parallel}$) or perpendicular ($\mathbf{q} = q_{\perp}$) to the film surface.

TABLE 1. Characteristics of Binary Particle/Polymer and Quasi-One-Component Particle-Brush Nanocomposites

sample ID	M_w (g/mol)[a] of grafts	M_w (g/mol)[b] of matrix	w_{NP} (%)[c]	w_{SiO_2} (%)[d]	φ (%)[e]	h (nm)[f]
SiO_2-S150	15 550		100.0	30.00	13.86	221 ± 10
SiO_2-S770	80 400		100.0	12.00	5.00	227 ± 15
S150/PS52k	15 550	52 000	33.0	10.00	4.03	284 ± 10
S770/PS52k	80 400	52 000	10.0	1.20	0.49	175 ± 10

[a] Molar mass of tethered PS. [b] Molar mass of homopolymer PS matrix. [c] Mass fraction of PS-grafted silica particles. [d] Mass fraction of silica core particles. [e] Volume fraction of silica core particles. [f] Film thickness of the samples.

The unique capability of our BLS to probe the direction dependent elastic properties without perturbation of the sample structure facilitates novel insights into the effect of molecular architecture on the mechanics of nanocomposite thin films. In particular, a pronounced anisotropy of phonon propagation is observed for particle-brush systems that contrasts the isotropic characteristics of classical composites based on binary polymer/nanoparticle blends. The anisotropy of phonon propagation in particle-brush systems is interpreted as a consequence of substrate-induced order formation of the particle brushes into layer-type structures that break the symmetry of the film. The results highlight the relevance of molecular architecture on the properties of polymer nanocomposites and suggest new opportunities to engineer quasi-one-component nanocomposites with advanced control of structural and property characteristics based on the assembly of particle-brush materials.

RESULTS AND DISCUSSION

The system in our study consists of binary blends of polystyrene and polystyrene-grafted silica nanoparticles as well as neat polystyrene-grafted silica particle thin films. The average particle (core) radius was determined by transmission electron microscopy (TEM) as $r_0 = 7.7 \pm 2$ nm, and surface-initiated atom transfer radical polymerization (SI-ATRP) was applied to synthesize particle model systems with the following graft characteristics: $\sigma = 0.84$ nm^{-2}, $N = 149$, $M_w/M_n = 1.21$ (sample ID: SiO_2-S150); $\sigma = 0.5$ nm^{-2}, $N = 773$, $M_w/M_n = 1.32$ (sample ID: SiO_2-S770). Here, σ denotes

the density, M_w/M_n is the distribution of graft molecular weights, and N is the degree of polymerization of surface-grafted chains. Binary particle composites were prepared by dispersion of appropriate amounts of PS-grafted particles within linear PS ($N = 500$, $M_n = 52$ kg/mol). Films were prepared by spin coating and subsequent thermal annealing at $T = 120$ °C for 24 h. The characteristics of binary polymer/particle blend and particle-brush systems are summarized in Table 1.

To determine the microstructure of the binary and particle−brush nanocomposite materials the particle dispersion morphology of all samples was determined using electron microscopy as shown in Figure 2. As revealed by the micrographs of bulk samples shown in Figure 2a,c (and in agreement with prior theoretical predictions), both particle systems (SiO_2-S770 and SiO_2-S150) are compatible with the polystyrene (PS) host polymer.[17,27,28]

The particle dispersion is also illustrated by cross-sectional images of the thin film samples shown in Figure 2b,d that reveal the homogeneous distribution of particles across the film transverse direction. In contrast, a more organized arrangement of particles is observed for SiO_2-S770 and SiO_2-S150 particle-brush samples both in-plane (Figure 2e,g) as well as normal to the film direction (Figure 2f,h) that suggests short-range order as well as accumulation of particle centers near the film interface. The structure formation in particle-brush systems will be discussed in more detail in the context of the elastic properties of particle-brush films.

Elastic Properties along In-Plane Film Direction. Figure 3 depicts representative BLS spectra $I(q,\omega)$ obtained in VV-polarized transmission geometry (see Figure 1a) to probe in-plane elastic excitations in SiO_2-S150 (see Figure 3a) and SiO_2-S150/PS (see Figure 3b) at wave vectors $q_\parallel = 0.0118$ and 0.0167 nm^{-1}, respectively. The amplitude of the wave vector $q_\parallel$ is determined and tuned by the scattering angle (see Methods section). For better visualization, the central Rayleigh peak around 6 GHz has been omitted in both spectra.

From the experimental data the frequencies corresponding to Brillouin peaks are determined by curve-fitting with a Lorentzian function. The observed Brillouin lines reveal the various film-guided phonons consistent with expectations for thin film samples with $q_\parallel \cong h^{-1}$. As in the simplified case of a homogeneous and isotropic plate, these phonons exhibit, along any direction parallel to the film, the form of plane waves propagating with a wave vector $q_\parallel$; along the normal direction they have to respect the boundary conditions applied on both surfaces of the film (see next section). The film-guided modes are confined within the film, reflected back and forth between the two plate surfaces. Of course they can leak into the surrounding media (air and/or glass substrate). The film-guided modes are polarized in the sagittal plane defined by the normal to the film and $q_\parallel$, having a mixed longitudinal-transverse character, in analogy to the well-known corresponding case of generalized Lamb modes of homogeneous and isotropic plates (see discussion below).[31] Their major characteristic is that, in contrast to the linear ($\omega = cq_\parallel$) relationship expected for acoustic-like phonons, these film-guided modes are dispersive: the phase velocity $c = \omega_i/q_\parallel$ depends on $q_\parallel$, where $\omega_i = 2\pi f_i$ is determined by the respective frequency f_i of the spectral peaks. Cheng *et al.* demonstrated that the identification of the various modes proceeds through the calculation of the dispersion relation f *versus* q which requires q-dependent measurements of $I(q,\omega)$.[29] The frequencies of film-guided modes usually fall between the transverse phonons in

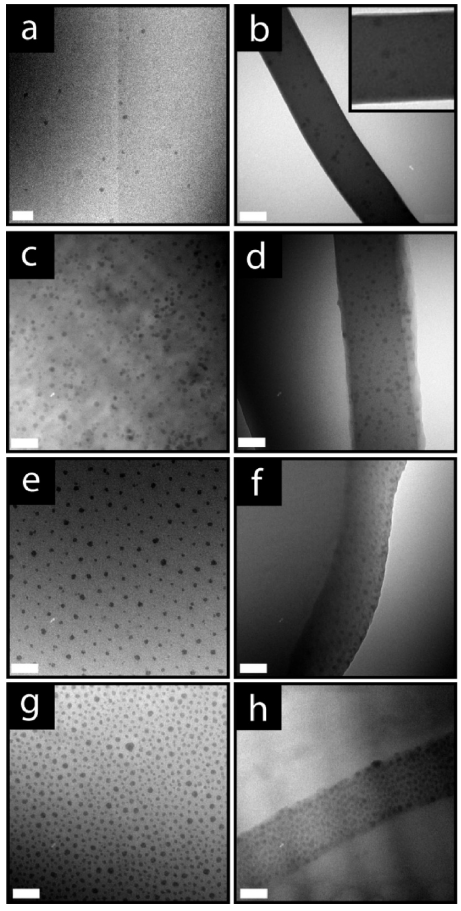

Figure 2. Transmission electron micrographs revealing microstructure of nanocomposite films after 24 h of thermal annealing at $T = 120$ °C. (a) Cross-sectional TEM of SiO_2-S770/PS bulk sample revealing uniform particle dispersion. (b) Cross-sectional TEM of SiO_2-S770/PS thin film confirming uniform particle dispersion. Inset shows magnification. (c) Cross-sectional TEM of SiO_2-S150/PS bulk sample revealing uniform particle dispersion. (d) Cross-sectional TEM of SiO_2-S150/PS thin film confirming uniform particle dispersion. (e) Top-view of SiO_2-S770 particle film (approximately monolayer). (f) Cross-sectional TEM of SiO_2-S770 particle thin film (approximately eight particle layers). (g) Top-view of SiO_2-S150 particle film (approximately monolayer). (h) Cross-sectional TEM of SiO_2-S150 particle thin film (approximately 15 particle layers). Scale bar is 100 nm.

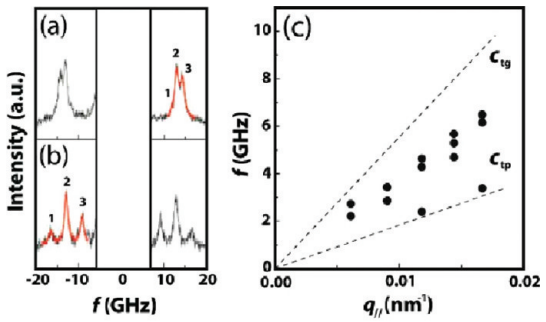

Figure 3. (a,b) Polarized (VV) BLS spectra of SiO_2-S150 film for in-plane phonon propagation at a scattering wave vector $q_{\parallel} = 0.0118$ nm^{-1} and SiO_2-S150/PS film at $q_{\parallel} = 0.0167$ nm^{-1}. Red lines represent Lorentzian fits. (c) Dispersion relation f *versus* $q_{\parallel}$ for SiO_2-S150 supported film. The two dashed lines indicate the transverse modes in the glass substrate (c_{tg} = 3390 m/s) and the bulk neat PS (c_{tp} = 1150 m/s).

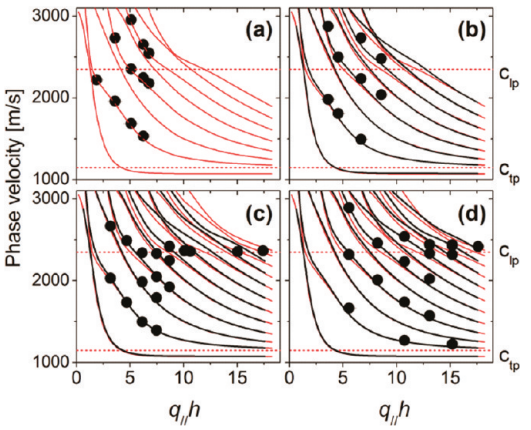

Figure 4. Phase velocity of the in-plane elastic excitations with wave vector $q_{\parallel}$ in the supported nanocomposite films of SiO_2-S770/PS (a) and SiO_2-S150/PS (b) and the supported particle films of SiO_2-S770 (c) and SiO_2-S150 (d) at ambient temperature. The solid symbols and lines correspond to the experimental data and the theoretical predictions for the propagation of the general Lamb modes, respectively. The red solid lines represent the theoretical dispersion relations of a neat PS, the solid black lines are the best theoretical fit to the experimental modes, and the dashed lines denote the phase velocities (c_{lp} and c_{tp}) for linear polystyrene.

bulk PS and glass (or generally the substrate), as indicated in the dispersion plot of SiO_2-S150 film in Figure 3c by the two dashed lines with the experimentally determined phase velocities c_{tp} = 1150 m/s and c_{tg} = 3390 m/s, respectively.

It has been well established that the surface excitations probed by BLS in thin films are the guided Lamb modes that can be calculated using a single set of bulk elastic parameters, with no adjustable parameters.[30,31] For supported PS films, the numerous guided modes have been well represented by the theoretical calculations using the values of the transverse (c_t) and longitudinal (c_l) phase velocities of bulk PS, glass and air as well as their densities (ρ).[31] We note that the calculation of the dispersion in the present films is based on the assumption that the structure is homogeneous on the length scales probed by the BLS experiment ($2\pi/q_{\parallel} \cong$ 200 nm). Figure 4 compares the experimental and calculated dispersion diagrams for all nanocomposite thin film samples. The diagrams display the phase velocity $\omega/q_{\parallel}$ as a function of $q_{\parallel}h$ (*i.e.*, the product of the wavenumber and the film thickness) as it is the relative magnitude of the phonon wavelength $2\pi/q_{\parallel}$ and the film thickness that determine the details of the film-guided modes. In Figure 4 the red solid lines represent the theoretical dispersion relations ($\omega/q_{\parallel}$ *versus* $q_{\parallel}h$) for the guided Lamb modes in a neat PS film, and the horizontal dashed lines represent the elastic sound phase velocities c_{lp} (= 2350 m/s) and c_{tp} determined for a thick ($q_{\parallel}h > 50$) PS film, that is, when the phonon wavelength becomes sufficiently shorter than the film thickness. The solid black lines present the best theoretical fit to the experimental modes.

Figure 4a reveals that the experimental dispersion relations of the polymer/particle binary blend film SiO_2-S770/PS are well captured by the theoretical predictions (red lines with fixed ρ_p, c_{lp}, and c_{tp} to their values in PS). The excellent agreement between theoretical and experimental values supports the assumption of isotropic elastic characteristics of both film samples consistent with the homogeneous morphology on the probed length scales. This is in accord with the expectation that no significant property changes are expected at small concentrations of inorganic additive ($w_{SiO_2} = 0.012$ for SiO_2-S770/PS). For the binary particle polymer film SiO_2-S150/PS with $w_{SiO_2} \approx 0.1$, Figure 4b suggests that the theoretical dispersion (solid black lines) better captures the experiment when assuming $c_{\parallel}$ ($\cong 1.04c_{lp}$) rather than c_{lp} of neat PS (red solid lines) thus indicating "stiffening" of the film associated with particle addition. Interestingly, the experimental dispersion curves are found to deviate significantly from the theoretical prediction for both particle-brush samples SiO_2-S770 (Figure 4c) and SiO_2-S150 (Figure 4d); the deviation increases with inorganic content. Since for sample SiO_2-S770 the composition is nearly identical to the binary nanocomposite SiO_2-S150/PS ($\phi \cong 0.1$) the disagreement between calculated and experimental values suggests that the assumption of structural and mechanical uniformity on probing length scales is not applicable in the case of particle-brush systems. This is an unexpected result since the dimensions of individual brush particles are only a small fraction of the probing phonon wavelengths and confirm that particle interactions have a prominent influence on the elastic characteristics of particle-brush thin films. In the following section it will be shown that the elastic properties of particle-brush films are indeed anisotropic.

Elastic Properties in Out-of-Plane Film Direction. Figure 5 depicts the BLS spectra for SiO_2-S150 and SiO_2-S150/PS recorded at a transverse scattering wave vector (see Figure 1b) of magnitude $q_{\perp} = 0.035$ nm^{-1} (corresponding

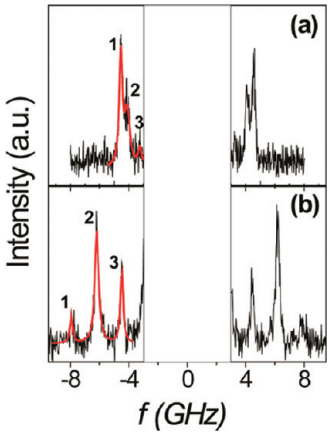

Figure 5. Polarized BLS spectra measured in reflection geometry for SiO_2-S150 (a) and SiO_2-S150/PS (b) films for out-of-plane phonon propagation at $q_\perp = 0.035$ nm^{-1}. The red lines represent Lorentzian fits.

to a probing length $2\pi/q_\perp \cong 170$ nm). Similar to the results of in-plane scattering geometry—but because of a different physical reason—a multimodal shape of the spectra is observed. The resolved peaks correspond to generalized Lamb modes representing standing acoustic excitations normal to the surface of the film where the parallel wave vector component $q_\parallel = 0$. This is consistent with the thin film sample geometries ($2\pi/q_\perp \cong h$) for which a splitting of the (single) longitudinal acoustic mode at $\omega = c_{lp}q_\perp$ (that is observed for films thicker than 2 μm) into a set of equidistant submodes is expected.[30]

The splitting can be understood to be a consequence of the formation of standing waves of acoustic excitations bounded by the film substrate and film free surface and the uncertainty $\Delta q \cong 2\pi/h$. The criterion for the formation of a standing wave of the order m is given by

$$q_m h = \pi m + \pi/2 \quad (1)$$

where m is an integer and $\pi/2$ is the phase shift due to the reflection on the film boundaries. The standing wave formation and the increasing distribution Δq with decreasing film thickness gives rise to the splitting into submodes that occupy the envelope of the broadened (bulk) longitudinal acoustic phonon mode. The frequency interval Δf_m between the peaks of the longitudinal submodes can be obtained directly from eq 1 as

$$\Delta f_m = c_\perp/(2h) \quad (2)$$

Note that from eq 2 the frequency splitting Δf_m between the adjacent modes of the BLS spectra (such as Figure 5) is directly related to the longitudinal sound velocity $c_\perp$ normal to the surface of the film. Figure 6 depicts the obtained sound velocities c_l for all polymer composite film samples along the in-plane and out-of-plane directions as a function of the weight fraction of the inorganic component.

Consistently, the effective sound velocity c_l normal to the film surface (open symbols) is found to be

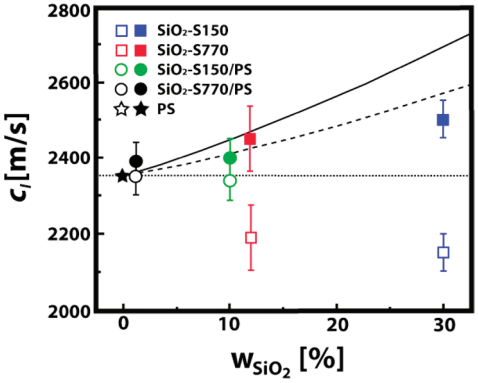

Figure 6. Comparison of the longitudinal phase velocity measured in the particle-brush and binary particle/polymer nanocomposite thin films revealing anisotropic phonon propagation ($c_\parallel > c_\perp$) in particle-brush systems. Blue squares, SiO_2-S150; red squares, SiO_2-S770; green circles, SiO_2-S150/PS; black circles, SiO_2-S770/PS. Solid and open symbols represent in-plane and out-of-plane elastic wave propagation, respectively. The star symbol corresponds to PS thin film (no anisotropy). Solid and dotted lines represent the effective medium prediction for parallel (in-plane) and normal (out-of-plane) configuration, respectively ($c_\parallel = c_{SiO_2}\phi_{SiO_2} + c_{PS}(1-\phi_{SiO_2})$ and $c_\perp^{-1} = (\phi_{SiO_2}/c_{SiO_2})^{-1} + [(1-\phi_{SiO_2})/c_{PS})]^{-1}$ (see ref 30). The phase velocity of the constituents is assumed to be $c_l = 4000$ m/s (SiO_2) and $c_l = 2350$ m/s (PS), respectively.[32,33]

smaller than its in-plane counterpart (solid symbols). However, whereas the splitting is small (within the experimental error) for binary particle/polymer blends, significant disparity between the in-plane and out-of-plane c_l is observed for both particle-brush systems; the anisotropy is found to increase with increasing concentration of inorganic component (no anisotropy was observed for neat PS that is represented by the horizontal dotted line). Note that the splitting in the case of SiO_2-S770 contrasts to the isotropic (within the experimental error) characteristics of the binary composite system SiO_2-S150/PS that exhibits near identical composition (~10 wt % SiO_2).

Strong directional dependence of longitudinal and transverse sound velocity has been recently reported for highly anisotropic polyimide coatings.[34] However, in the present case all samples are in their quiescent state. Prior to a rationalization of the unprecedented mechanical anisotropy of the present polymer nanocomposite films, we should first recall the two main channels for structural information in such nonperiodic systems from the BLS spectra: first, the presence of boundaries with elastic impedance contrast (density, sound velocities) and, second, heterogeneities with length scales larger than the probing phonon wavelength. We attribute the splitting of c_l in Figure 6 to the interaction between the particle brushes and the substrate that gives rise to a layer-type organization of particles near the interface and thus results in breaking of the symmetry of the film. This argument is supported by Figure 7 that provides a comparison of the spatial distribution of particle cores in the out-of-plane

direction for both the SiO_2-S150/PS and SiO_2-S770 composite systems (both with weight fraction of inorganic component of about $w_{SiO_2} = 0.1$).

The particle counting analysis shown in Figure 7c confirms that in the case of the particle-brush sample SiO_2-S770 the particle cores concentrate along the substrate resulting in alternating regions of high and low particle density in the vertical film direction (analogous ordering is observed for SiO_2-S150 particle-brush films, see Figure 2h); a close-packing configuration (as indicated in the inset to Figure 7a) would imply an interparticle distance of $\sqrt{3}R \cong 44$ nm along the vertical (out-of-plane) direction, in good agreement with the experimental value of about 40 nm. The degree of order formation in vertical direction is found to decay with increasing distance from the substrate and a more randomized distribution (comparable to the bulk structure of the film) is observed at distances corresponding to about four particle diameters (approximately 150 nm). The layer-type organization of particle centers contrasts the uniform particle distribution that is observed in the binary composite system SiO_2-S150/PS as shown in Figure 2d,f. Figure 7a also reveals the apparent concentration of the particle centers in the vicinity of the substrate in the SiO_2-S770 thin film. This observation was found to be independent of tilt-orientation and thus cannot be attributed to an imaging artifact. We interpret the apparent depletion of polymer grafts from the vicinity of the substrate to be a consequence of repulsive polymer–substrate interactions that originate from the confining effect that the substrate exerts on the grafted polymer chains. Because for polymer brushes the grafting of one chain end imparts additional constraints on the conformation of the polymer chain, we expect that the confinement effect imparted by the substrate is more pronounced for particle-brush systems as compared to the binary particle/polymer blend system. An alternative (enthalpy dominated) driving force for the interfacial segregation of particle cores could be provided by the residual interaction between the silica particle cores and the (silica) substrate facilitated through only partial screening of the inorganic core. However, given the similar and dense grafting of polymer chains in both particle-brush systems (σ = 0.84 nm^{-2} and σ = 0.5 nm^{-2} for SiO_2-S150 and SiO_2-S770, respectively) core-substrate interactions are expected to be effectively screened out in both particle systems. The latter assumption is supported by the absence of any segregation in the SiO_2-S150/PS (and similarly SiO_2-S770/PS) system that, in the case of enthalpy dominated segregation, should behave similarly to the quasi-one-component SiO_2-S770 system.

We hypothesize that the particle organization imparts a layer-type modulation of stiffness within the particle-brush film that results in distinct phonon propagation characteristics of in-plane and out-of-plane direction. Specifically, we expect the depletion of polymer grafts from the surface (that can be discerned from the micrographs such as Figure 7a) to result in the softening of the interfacial layer because the increased concentration of chain ends between the first and second particle layer should accelerate chain dynamics.[35] Support for this interpretation is provided by recent numerical simulations of the local mechanical properties of particle-filled polymers that have revealed repulsive filler–matrix interactions to result in the lowering of the glass transition temperature in the vicinity regions of particle fillers.[36] Since the phonon propagation along out-of-plane direction is sensitive to the presence of soft interlayers, a reduction of $c_\perp$ in out-of-plane direction is thus expected.[37] However, the observed drop with increasing SiO_2 particle volume

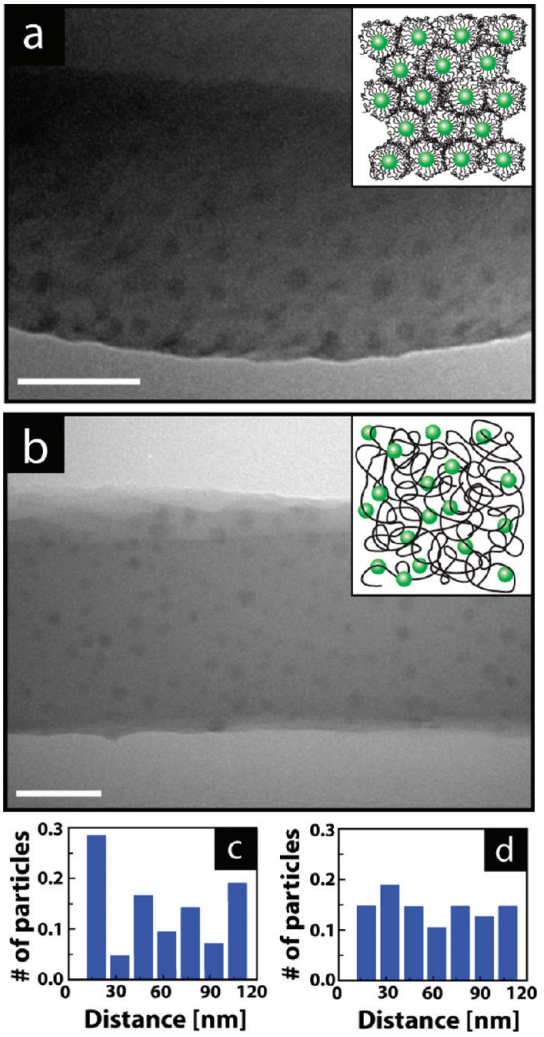

Figure 7. Cross-sectional TEM and image analysis revealing layer-type particle organization in particle-brush thin films: (a) SiO_2-S770; (b) SiO_2-S150/PS. In both micrographs the lower film surface is oriented toward the substrate. (c,d) Out-of-plane particle distribution (distance is with respect to the substrate interface) revealing layer-type organization for SiO_2-S770 (c) and uniform distribution for SiO_2-S150/PS (d). Scale bar is 100 nm.

fraction cannot be accounted for by the common effective medium relations (dotted and solid lines in Figure 6).[37,38] In contrast, phonon propagation along the in-plane film direction should be determined by the elastic properties of the bulk section of the film that is found to be in semiquantitative agreement with the effective medium prediction (dashed line) for both the particle-brush as well as binary particle/polymer blend systems (see Figure 6); the linear dependence $c_{||}(w_{SiO_2})$ (solid line) largely overestimates the experiment. The more significant deviation between the predicted and experimental phase velocities in the case of SiO_2-S150 is attributed to the short graft length and the CPB character of SiO_2-S150 that will act to reduce entanglement and thus reduce c_l below the expected value of neat PS.

Note that since vertical order extends only few particle diameters within the out-of-plane film direction and since the effect of particle ordering on the anisotropy of phonon propagation should depend on the volume fraction of the ordered region within the film, the anisotropy is expected to vanish in the limit of thick films. This trend is indeed observed in films of SiO_2-S770 as demonstrated in Figure 8 that depict the measured phonon propagation velocity in out-of-plane direction as a function of film thickness. The out-of-plane velocity is found to systematically converge to the respective bulk value with increasing film thickness; films in excess of 3 μm in thickness (corresponding to about 100 particle-brush layers) were found to be isotropic.

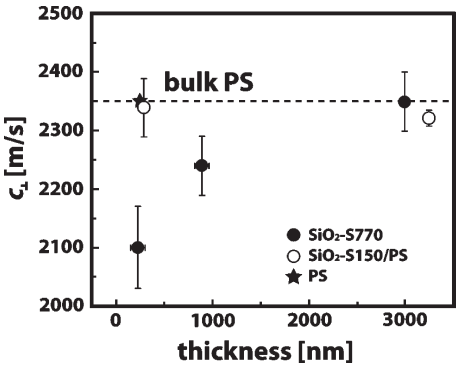

Figure 8. Dependence of the longitudinal phase velocity in out-of-plane direction on the thickness of SiO_2-S770 films revealing the decrease of anisotropy with increasing thickness of particle film. Dotted line indicates the phase velocity of the bulk PS film.

CONCLUSIONS

The assembly of polymer-grafted particles has been shown to provide a path to quasi-one-component nanocomposites with bulk elastic characteristics (in the GHz regime) similar to classical binary particle/polymer blends with corresponding characteristics (chain length and composition) of the respective constituents. The short-ranged organization of particle brushes near the substrate interface into layer-type structures gives rise to anisotropic elastic properties in thin film geometries that underline the relevance of particle-brush interactions on the mechanical properties of the (quasi-one-component) nanocomposites. The emergence of anisotropy also highlights novel opportunities for engineering polymer nanocomposites with advanced control of both the particle dispersion morphology as well as the associated physical properties based on particle-brush materials. These materials could find applications, for example, in actuators, robust self-assembled photonic crystals, directional sound limiters or—if the approach can be extended to semiconductor particle compositions—materials for solid state lighting. To harness the particle-brush approach as a route toward "precision engineered polymer nanocomposites", better understanding of the interrelation between brush architecture and the macroscopic mechanical characteristics of particle-brush assemblies, such as Young's modulus, yield strength, and toughness will be essential. The evaluation of these parameters is the subject of our current research.

METHODS

Particle Synthesis. The synthesis of SiO_2-S150 and SiO_2-S770 particle-brush systems was performed using surface-initiated atom-transfer radical polymerization (SI-ATRP) as described in a previous publication.[39,40] Polystyrene with (number-average) molecular weight M_n = 52000 g/mol (polydispersity index M_w/M_n = 1.02) was obtained by Polymer Source and used as received. Toluene solvent was obtained by Aldrich and used without further purification. The particle dimensions were evaluated by transmission electron microscopy (TEM) in the dry state as well as by photon correlation spectroscopy in dilute solution. The geometric and hydrodynamic radii were determined as R = 20 nm and R_h = 29 nm for SiO_2-S150 as well as R = 27 nm and R_h = 67 nm for SiO_2-S770, respectively.[25] From $R/R_h \cong 0.68$ (SiO_2-S150) and $R/R_h \cong 0.4$ (SiO_2-S770) the particle systems can be assigned to the CPB (SiO_2-S150) and SDPB (SiO_2-S770) regimes.

Film Preparation and Analysis. Film thickness and composite morphology were determined by cross-sectional TEM of the layer (the particle or the particle-filled polymer film) sandwiched between poly(acrylic acid) (PAA) layers. Nanocomposite thin films of about 300 nm thickness were obtained by spin-coating a 3% particle/polymer solution in toluene on a PAA substrate and subsequent thermal annealing. PAA film was then placed on top of the nanocomposite layer by spin-coating, creating a sandwich structure. Films were microsectioned at room temperature using a LEICA EM FCS cryo-ultra microtome. Spatial distribution of the particles across the films was analyzed using ImageJ software. Table 1 presents a summary of the thickness and composition of the particle and the particle filled polymer films used in the present study.

BLS Spectroscopy. Brillouin light scattering was used in order to evaluate the elastic properties of nanocomposite thin films because of several reasons: (1) it is a nondestructive technique that allows for mechanical and subsequent structural characterization of thin film samples and (2) it provides access to both in-plane and out-of plane elastic properties by virtue of the scattering geometry that is being used.[29,30,34,41,42] Furthermore,

BLS provides information about elastic properties at hypersonic frequencies (GHz regime) that are more sensitive to local packing and interactions within the test material. In contrast to the usually encountered backscattering geometry for film samples, the present BLS setup allows q dependent measurements as described in our previous studies.[29,30] The scattering configuration is depicted in Figure 1. In the transmission geometry (see Figure.1a) with a scattering angle θ (=2α) twice the reflection angle α, the scattering wave vector **q** is parallel to the film and its magnitude $q_{\parallel} = (4\pi/\lambda)\sin(\theta/2)$ is independent of the medium refractive index; λ = 532 nm is the wavelength of the incident laser beam. In the reflection geometry (see Figure.1b) with the scattering angle $\theta = \pi - 2\alpha$; **q** is normal to the film surface with magnitude $q_{\perp} = (4\pi n/\lambda)\sin(\theta/2)$, n being the medium refractive index. Using these special two geometries, BLS facilitates the selective probing of phonons (thermal density fluctuations) propagating either parallel (in plane) or normal (out-of-plane) to the film. The spectrum of the inelastically scattered light is analyzed by a high resolution (3 + 3)-pass tandem Fabry−Perot interferometer (FPI) (JRS Instruments, Switzerland) at hypersonic frequencies (1−50 GHz). Choosing the polarization of both incident laser beam and scattered light was selected polarized normal to the scattering plane (perpendicular to the film) the polarized spectrum $I(q,\omega)$ with angular frequency $\omega = 2\pi f$ can be recorded. All BLS experiments were performed at room temperature (T = 23 °C). BLS emerges as a powerful technique for recording the dispersion diagram of structured nanocomposites.[41,42]

Theoretical calculations. For the theoretical predictions of the dispersion plots we used the layered-multiple-scattering method for elastic waves appropriately adapted to calculate the eigenmodes for layered structures composed by homogeneous and isotropic plates free or supported on a substrate.[43] The method, in its general form, evaluates rigorously the elastic properties of composite systems consisting of a number of different layers having the same two-dimensional periodicity in the plane parallel to the layers, while no periodicity is required in the direction perpendicular to them. Here, the procedure was applied for the simple case where all layers are homogeneous plates, following the technique described in ref 29 for the calculation of the dispersion plots $\omega(q_{\parallel})$, with $q_{\parallel}$ being the wave vector parallel to the planes.

Electron Microscopy. TEM was performed using a JEOL EX2000 electron microscope operated at 200 kV. Images were taken using a Gatan Orius SC600 high-resolution camera.

Acknowledgment. M.R.B. acknowledges financial support by the Air Force Office for Scientific Research (*via* Grant FA9550-09-1-0169) and the National Science Foundation (*via* Grant DMR-1006473). P.V. and G.F. thank GRST (Grant PENED 2003/856) and EU-NANODIRECT (CP F213948-2) for financial support.

REFERENCES AND NOTES

1. Winey, K. I.; Vaia, R. A. Polymer Nanocomposites. *MRS Bull.* **2007**, *32*, 314–319.
2. Fukushima, Y.; Inagaki, S. Synthesis of an Intercalated Compound of Montmorillonite and 6-Polyamide. *J. Inclusion Phenom.* **1987**, *5*, 473–482.
3. Usuki, A.; Kawasumi, M.; Kojima, Y.; Okada, A.; Kurauchi, T.; Kamigaito, O. Swelling Behavior of Montmorillonite Cation Exchanged for Omega-Amino Acids by Epsilon-Caprolactam. *J. Mater. Res.* **1993**, *8*, 1174–1178.
4. Giannelis, E. P. Polymer Layered Silicate Nanocomposites. *Adv. Mater.* **1996**, *8*, 29–35.
5. Vaia, R. A.; Maguire, J. F. Polymer Nanocomposites with Prescribed Morphology: Going Beyond Nanoparticle-Filled Polymers. *Chem. Mater.* **2007**, *19*, 2736–2751.
6. Bockstaller, M. R.; Mickiewicz, R. A.; Thomas, E. L. Block Copolymer Nanocomposites: Perspectives for Tailored Functional Materials. *Adv. Mater.* **2005**, *17*, 1331–1349.
7. Vaia, R. A.; Wagner, H. D. Framework for Nanocomposites. *Mater. Today* **2004**, *7*, 32–37.
8. Vaia, R. A.; Ishii, H.; Giannelis, E. P. Synthesis and Properties of 2-Dimensional Nanostructures by Direct Intercalation of Polymer Melts in Layered Silicates. *Chem. Mater.* **1993**, *5*, 1694–1696.
9. Ray, S. S.; Okamoto, M. Polymer/Layered Silicate Nanocomposites: A Review from Preparation to Processing. *Prog. Polym. Sci.* **2003**, *28*, 1539–1641.
10. Bockstaller, M.; Kolb, R.; Thomas, E. L. Metallodielectric Photonic Crystals Based on Diblock Copolymers. *Adv. Mater.* **2001**, *13*, 1783–1786.
11. Bockstaller, M. R.; Thomas, E. L. Proximity Effects in Self-Organized Binary Particle-Block Copolymer Blends. *Phys. Rev. Lett.* **2004**, *93*, 166106.
12. Ray, S. S.; Bousmina, M. Polymer Nanocomposites and Their Applications; American Scientific: Stevenson Ranch, CA, 2006.
13. Arbatti, M.; Shan, X. B.; Cheng, Z. Y. Ceramic-Polymer Composites with High Dielectric Constant. *Adv. Mater.* **2007**, *19*, 1369.
14. Krishnamoorti, R.; Vaia, R. A., Eds. *Polymer Nanocomposites: Synthesis Characterization and Modeling*; ACS Symposium Series; American Chemical Society: Washington DC, 2001.
15. Mackay, M. E.; Tuteja, A.; Duxbury, P. M.; Hawker, C. J.; Van Horn, B.; Guan, Z. B.; Chen, G. H.; Krishnan, R. S. General Strategies for Nanoparticle Dispersion. *Science* **2006**, *311*, 1740–1743.
16. Borukhov, I.; Leibler, L. Enthalpic Stabilization of Brush-Coated Particles in a Polymer Melt. *Macromolecules* **2002**, *35*, 5171–5182.
17. Harton, S. E.; Kumar, S. K. Mean-Field Theoretical Analysis of Brush-Coated Nanoparticle Dispersion in Polymer Matrices. *J. Polym. Sci., Polym. Phys.* **2008**, *46*, 351–358.
18. Akcora, P.; Liu, H.; Kumar, S. K.; Moll, J.; Li, Y.; Benicewicz, B. C.; Schadler, L. S.; Acehan, D.; Panagiotopoulos, A. Z.; Pryamitsyn, V. *et al.* Anisotropic Self-Assembly of Spherical Polymer-Grafted Nanoparticles. *Nat. Mater.* **2009**, *8*, 354–U121.
19. Akcora, P.; Kumar, S. K.; Moll, J.; Lewis, S.; Schadler, L. S.; Li, Y.; Benicewicz, B. C.; Sandy, A.; Narayanan, S.; Illavsky, J. *et al.* "Gel-like" Mechanical Reinforcement in Polymer Nanocomposite Melts. *Macromolecules* **2010**, *43*, 1003–1010.
20. Theoretical studies have shown that in athermal polymer/particle blends the formation of stable particle dispersion is only expected if (a) the particle diameter is much less than the radius of gyration of the host polymer (see ref 15) or (b) the particle is grafted with polymer chains such that the degree of polymerization of surface-grafted chains is large enough to permit swelling of the brush by matrix chains (the so-called "wet brush regime", see also refs 16 and 17). Both conditions lead to unfavorable constraints with regard to technological applications of nanocomposites due to limitations of particle size or the maximum attainable inorganic filling fraction.
21. Choi, J.; Dong, H.; Matyjaszewski, K.; Bockstaller, M. R. Flexible Particle Array Structures by Controlling Polymer Graft Architecture. *J. Am. Chem. Soc.* **2010**, *132*, 12537–12539.
22. Ohno, K.; Morinaga, T.; Takeno, S.; Tsujii, Y.; Fukuda, T. Suspensions of Silica Particles Grafted with Concentrated Polymer Brush: Effects of Graft Chain Length on Brush Layer Thickness and Colloidal Crystallization. *Macromolecules* **2007**, *40*, 9143–9150.
23. Dukes, D.; Li, Y.; Lewis, S.; Benicewicz, B.; Schadler, L.; Kumar, S. K. Conformational Transitions of Spherical Polymer Brushes: Synthesis, Characterization, and Theory. *Macromolecules* **2010**, *43*, 1564–1570.
24. Pietrasik, J.; Hui, C. M.; Chaladaj, W.; Dong, H.; Choi, J.; Jurczak, J.; Bockstaller, M. R.; Matyjaszewski, K. Silica−Polymethacrylate Hybrid Particles Synthesized Using High-Pressure Atom Transfer Radical Polymerization. *Macromol. Rapid Commun.* **2011**, *32*, 295–301.
25. Voudouris, P.; Choi, J.; Dong, H.; Bockstaller, M. R.; Matyjaszewski, K.; Fytas, G. Effect of Shell Architecture on the Static and Dynamic Properties of Polymer-Coated Particles in Solution. *Macromolecules* **2009**, *42*, 2721–2728.
26. Tchoul, M. N.; Fillery, S. P.; Koerner, H.; Drummy, L. F.; Oyerokun, F. T.; Mirau, P. A.; Durstock, M. F.; Vaia, R. A. Assemblies of Titanium Dioxide-Polystyrene Hybrid

Nanoparticles for Dielectric Applications. *Chem. Mater.* **2010**, *22*, 1749–1759.
27. The grafting of polymer chains on spherical (curved) surfaces reduces chain crowding with increasing distance from the particle surface. This effect promotes swelling of the particle brush with matrix chains as compared to the planar brush analogue (see ref 17). Thus, the threshold degree of polymerization of surface-grafted chains to facilitate compatibilization in a matrix polymer of a given molecular weight increases with the grafting density or the particle radius of the particle brush. See also ref 28.
28. Kim, J.; Green, P. F. Phase Behavior of Thin Film Brush-Coated Nanoparticles/Homopolymer Mixtures. *Macromolecules* **2010**, *43*, 1524–1529.
29. Cheng, W.; Sainidou, R.; Burgardt, P.; Stefanou, N.; Kiyanova, A.; Efremov, M.; Fytas, G.; Nealey, P. F. Elastic Properties and Glass Transition of Supported Polymer Thin Films. *Macromolecules* **2007**, *40*, 7283–7290.
30. Gomopoulos, N.; Cheng, W.; Efremov, M.; Nealey, P. F.; Fytas, G. Out-of-Plane Longitudinal Elastic Modulus of Supported Polymer Thin Films. *Macromolecules* **2009**, *42*, 7164–7167.
31. Auld, B. A. *Acoustic Fields and Waves in Solids*; Wiley: New York, 1973; p 2v.
32. The c_l for silica (4000 m/s) is typical for colloidal silica (see ref 33).
33. Still, T.; Mattarelli, M.; Kiefer, D.; Fytas, G.; Montagna, M. Eigenvibrations of Submicrometer Colloidal Spheres. *J. Phys. Chem. Lett.* **2010**, *1*, 2440–2444.
34. Gomopoulos, N.; Saini, G.; Efremov, M.; Nealey, P. F.; Nelson, K.; Fytas, G. Nondestructive probing of mechanical anisotropy in polyimide films at nanoscale. *Macromolecules* **2010**, *43*, 1551–1555.
35. Lee, J. Y.; Su, K. E.; Chan, E. P.; Zhang, Q. L.; Ernrick, T.; Crosby, A. J. Impact of Surface-Modified Nanoparticles on Glass Transition Temperature and Elastic Modulus of Polymer Thin Films. *Macromolecules* **2007**, *40*, 7755–7757.
36. Papakonstantopoulos, G. J.; Yoshimoto, K.; Doxastakis, M.; Nealey, P. F.; de Pablo, J. J. Local Mechanical Properties of Polymeric Nanocomposites. *Phys. Rev. E.* **2005**, *72*, 031801.
37. Courtney, T. H. Mechanical Behavior of Materials, 2nd ed.; McGraw Hill: Boston, 2000; pp xviii, 733.
38. Maldovan, M.; Bockstaller, M. R.; Thomas, E. L.; Carter, W. C. Validation of the Effective-Medium Approximation for the Dielectric Permittivity of Oriented Nanoparticle-Filled Materials: Effective Permittivity for Dielectric Nanoparticles in Multilayer Photonic Composites. *Appl. Phys. B* **2003**, *76*, 877–884.
39. Jakubowski, W.; Min, K.; Matyjaszewski, K. Activators Regenerated by Electron Transfer for Atom Transfer Radical Polymerization of Styrene. *Macromolecules* **2006**, *39*, 39–45.
40. Bombalski, L.; Dong, H. C.; Listak, J.; Matyjaszewski, K.; Bockstaller, M. R. Null-Scattering Hybrid Particles Using Controlled Radical Polymerization. *Adv. Mater.* **2007**, *19*, 4486–4490.
41. Jang, J.-H.; Ullal, C. K.; Gorisshnyy, T.; Tsukruk, V. V.; Thomas, E. L. Mechanically Tunable Three-Dimensional Elastomeric Network/Air Structures *via* Interference Lithography. *Nano Lett.* **2006**, *6*, 741–743.
42. Sato, A.; Pennec, Y.; Shingne, N.; Thurn-Albrecht, T.; Knoll, W.; Steinhart, M.; Djafari-Rouhani, B.; Fytas, G. Tuning and Switching Hypersonic Phononic Properties of Elastic Impedance−Contrast Nanocomposites. *ACS Nano* **2010**, *4*, 3471–3481.
43. Sainidou, R.; Stefanou, N.; Psarobas, I. E.; Modinos, A. A Layer Multiple-Scattering Method for Phononic Crystals and Heterostructures of Such. *Comput. Phys. Commun.* **2005**, *166*, 197–240.